Supporting Information for
Discovery of Dramatically Improved Ammonia Synthesis Catalysts through Hierarchical High Throughput Catalyst Screening of the Fe(211) Surface

Jon Fuller[1], Alessandro Fortunelli[2,3*], William A. Goddard[2*], Qi An[1*]

[1]Department of Chemical and Materials Engineering, University of Nevada – Reno, Nevada 89577, United States

[2]Materials and Procs Simulation Center (MSC) California Institute of Technology, Pasadena, California 91125, United States

[3]CNR-ICCOM, Consiglio Nazionale delle Ricerche, ThC2-Lab, Pisa, 56124, Italy

*Corresponding authors email: qia@unr.edu, alessandro.fortunelli@cnr.it, wag@caltech.edu

Table of Contents:

Supplemental Data Items

Table S1-S2

Figure S1-S4

Table S1 Preferred doping positions of elements in the first and second layer of Fe(211)R. Positions are listed with (1st) or (2nd) layer followed by the specific position. I indicates surface issues in each position, shown in Fig. 1SI. Each element was found to have the lowest electronic energy in this position after optimization relative to the six distinct positions tested in the first and second layers shown in Fig. 1 (A).

Element	Doping Position	Element	Doping Position	Element	Doping Position
Co	(2nd) Bottom-left	Y	I	Ca	I
Cr	(2nd) Mid-right	Zr	(2nd) Mid-right	Mg	(2nd) Mid-left
Cu	(1st) Bottom	Au	(1st) Bottom	Sr	I
Mn	(2nd) Bottom-left	Hf	(2nd) Bottom-right	As	(2nd) Mid-right
Ni	(1st) Mid	Hg	I	Ge	(1st) Mid
Sc	(2nd) Bottom-right	Ir	(2nd) Bottom-left	Sb	(1st) Mid
Ti	(2nd) Bottom-right	Os	(2nd) Bottom-left	Si	(2nd) Mid-right
V	(2nd) Mid-right	Pt	(1st) Mid	Te	(1st) Mid
Zn	(2nd) Bottom-right	Re	(2nd) Bottom-left	Al	(2nd) Bottom-right
Ag	(2nd) Bottom-left	Ta	(2nd) Bottom-right	Bi	(1st) Mid
Cd	I	W	(2nd) Bottom-right	Ga	(2nd) Bottom-right
Mo	(2nd) Mid-right	La	(1st) Mid	In	(1st) Mid
Nb	(2nd) Mid-right	Eu	I	Pb	I
Pd	(1st) Bottom	Ce	I	Sn	I
Rh	(1st) Bottom	Dy	I	Tl	I
Ru	(2nd) Bottom-left	Ba	I		
Tc	(2nd) Bottom-left	Be	(1st) Mid		

Table S2 Lowest energy state for each element for third and fourth criterion comparison. The 4N** and 3N-NH-H states were found to be lower depending on each doped element; the preferred resting state for third criterion was determined based on the greatest dG for the high energy 3N-NH3-H state tested in the third criterion between either 3N-NH-H or 4N** for each element.

Element	3N-NH-H -> 3N-NH3-H dG (eV)	4N** -> 3N-NH3-H dG (eV)	Preferred Low Energy State
Co	1.43	1.36	3N-NH-H
Cr	1.51	1.61	4N**
Mn	2.02	1.90	3N-NH-H
Sc	1.46	1.59	4N**
Ti	1.55	1.51	3N-NH-H
V	1.00	1.49	4N**
Zn	1.93	1.75	3N-NH-H
Mo	1.65	1.69	4N**
Nb	1.33	1.06	3N-NH-H
Ru	1.42	1.56	4N**
Zr	1.31	1.41	4N**
Hf	1.59	1.88	4N**
Ir	1.34	1.63	4N**
Os	1.24	1.63	4N**
Pt	1.21	1.08	3N-NH-H
Ta	1.42	1.73	4N**
W	1.43	3.18	4N**
La	2.03	3.08	4N**
Al	1.45	1.61	4N**

Table S3 Convergence with respect to number of kMC steps for Fe-bcc(211)R and Co-doped bcc(211)R at T = 673 K, P = 15:5:1 atm H_2:N_2:NH_3 ; time listed in seconds while product is NH_3mol/s/(2×2).

kMC step amount	Time – Fe-bcc(211)R	Product – Fe-bcc(211)R	Time – Co-doped bcc(211)R	Product – Co-doped bcc(211)R
$4 * 10^8$	67.205	3.839	37.674	10.777
$4 * 10^9$	663.806	3.926	363.642	11.253
$4 * 10^{10}$	6616.703	3.829	3640.610	10.890
$4 * 10^{11}$	66133.123	3.853	3639.046	10.897
$4 * 10^{12}$	661353.498	3.846	364191.039	10.883

Be 4
Mg 12
Sc 21 Ti 22 V 23 Cr 24 Mn 25 Co 27 Ni 28 Cu 29 Zn 30 Ga 31 Ge 32 As 33 Al 13 Si 14
Zr 40 Nb 41 Mo 42 Tc 43 Ru 44 Rh 45 Pd 46 Ag 47 In 49 Sb 51 Te 52
Hf 72 Ta 73 W 74 Re 75 Os 76 Ir 77 Pt 78 Au 79 Bi 83
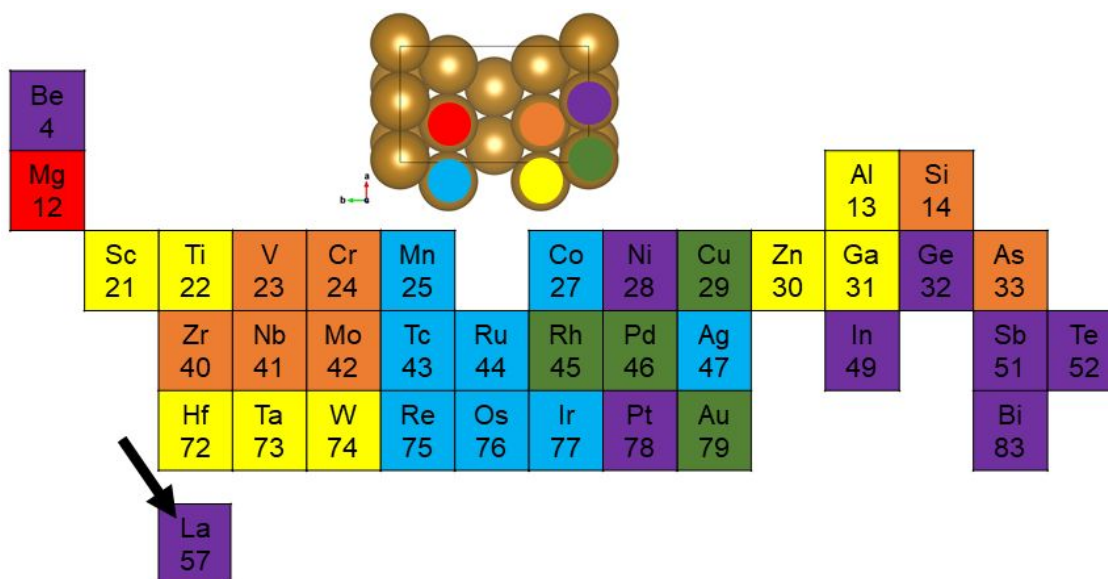La 57

Figure S1 Preferred positions of the 37 remaining HHTCS candidates after stability check (4N position shown in Fig 3). Doping positions are shown on the Fe(211)R surface in color at the top for clarity, with similar shading for each element.
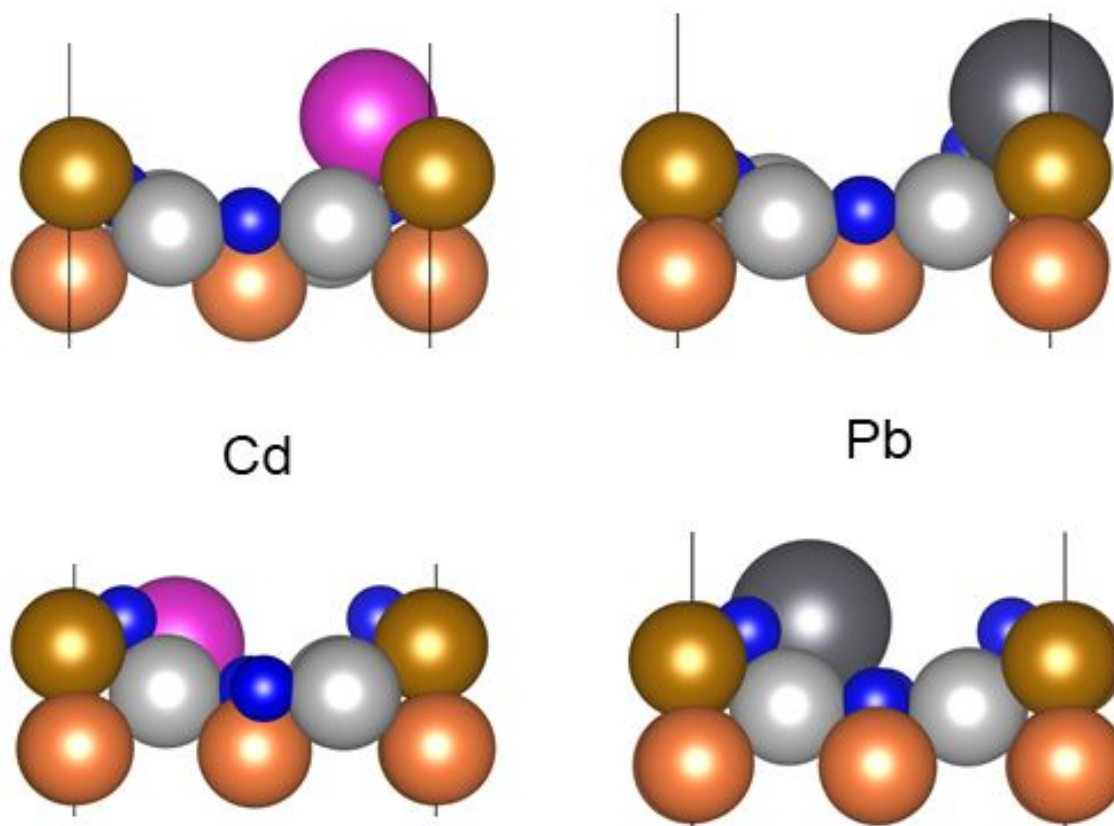
Figure S2 Side view of surface behavior of elements with issues during stability check prior to criterion 1. Large elements and several others exhibit rejection of position in surface, forming complexes with adsorbed N from trough region / threefold sites in second layer above the surface that are deemed prohibitive to the reaction mechanism. Cd, shown on the left, and Pb, shown on the right are two such elements; first layer behavior is shown on top and second layer behavior is shown on bottom.
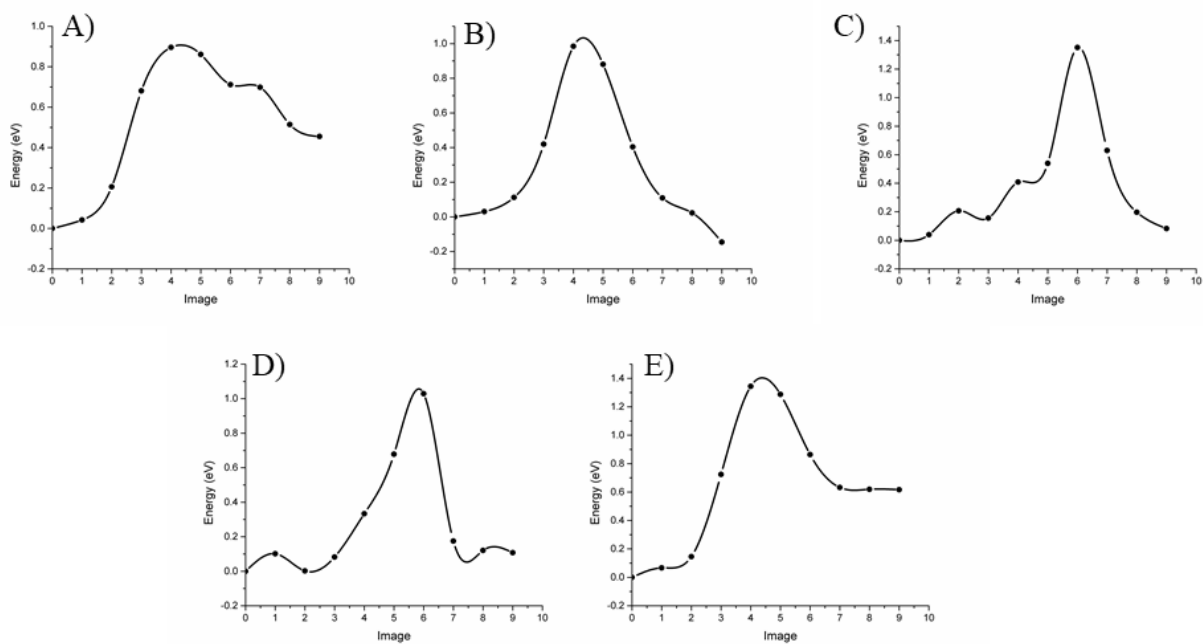
Figure S3 Climbing nudged elastic band (NEB) results for hydrogenation transition states are shown are shown above in terms of energy in eV. The NEB method generates a true transition state verified by phonon calculations identifying a single negative curvature in the Hessian. Dimer calculations were performed for all negative frequencies calculated from the NEB images. A) 3N-NH-H -> 3N-NH$_2$, B) 3N-NH$_2$-2H -> 3N-NH$_3$-H, C) 3N-H -> 2N-NH, D) 2N-NH-2H -> 2N-NH$_2$-H, E) 2N-NH$_2$-H -> 2N-NH$_3$.
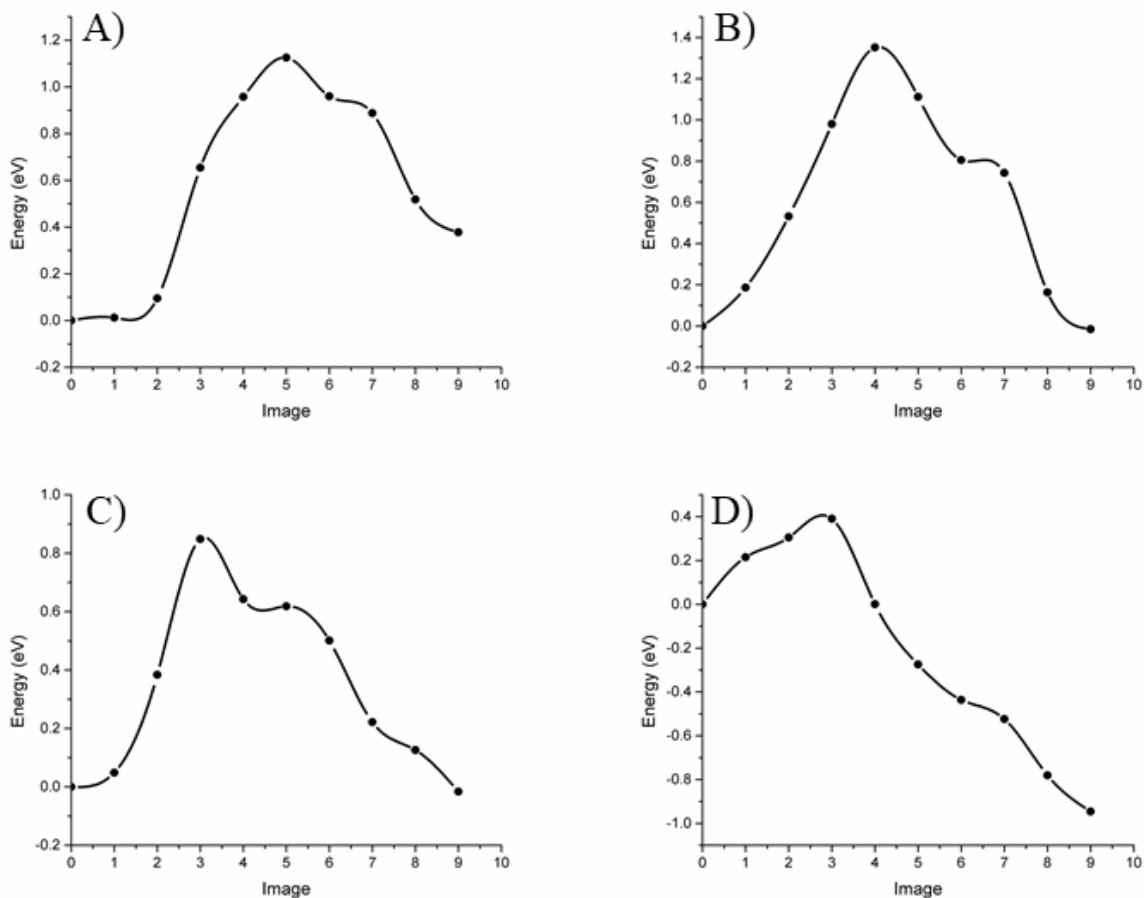
Figure S4 Climbing nudged elastic band (NEB) results for N_2 transition states in the complex N_2 dissociation pathway are shown are shown above in terms of energy in eV. The NEB method generates a true transition state verified by phonon calculations identifying a single negative curvature in the Hessian. Dimer calculations were performed for all negative frequencies calculated from the NEB images. A) 2N-2H-N2(top) -> 2N-2H-N2(bottom), B) 2N-2H-N2(bottom) -> 2N-2H-N2(F), C) 2N-2H-N2(F) -> 4N-2H, D) 4N initial -> 4N**.
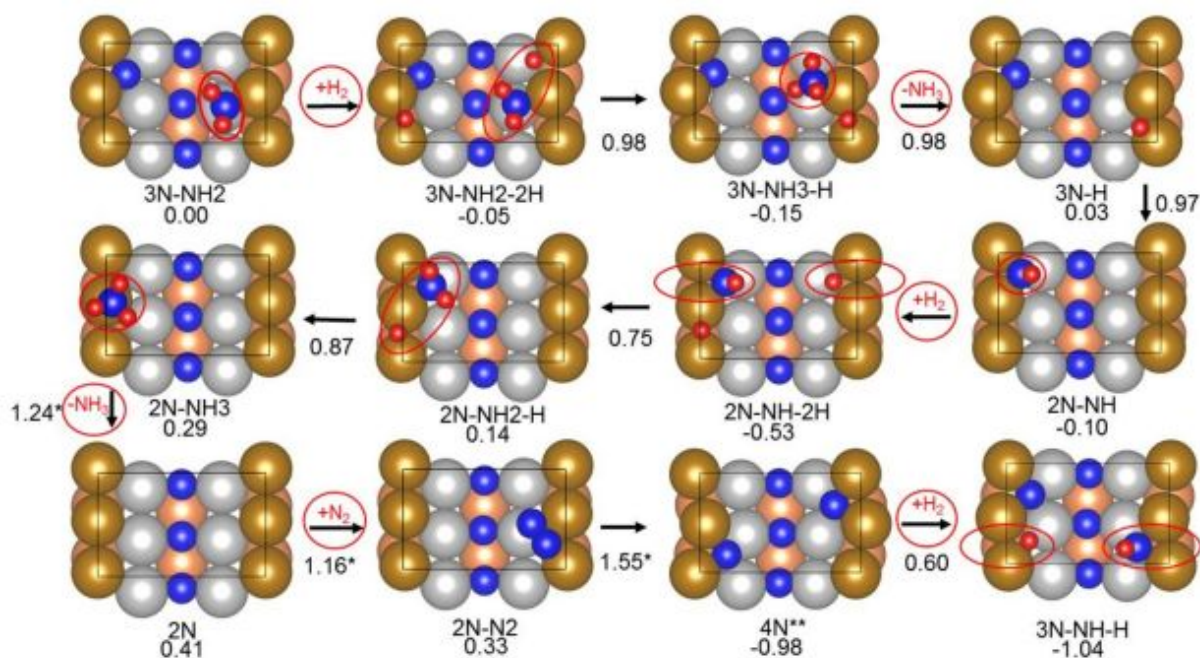
Figure S5 Full reaction pathway for Fe-bcc(211)R (taken from previous work published in Fuller et. al - Reaction mechanism and kinetics for ammonia synthesis on the Fe(211) reconstructed surface. *Phys. Chem. Chem. Phy.* **2019**, 21, 11444-11454). Energies given are in eV for distinct configurations and transitions; addition and removal of adsorbates are indicated between states and circled for clarity. * Full complex N_2 dissociation pathway is not shown, only important 2N-2H-N_2(F) state.